Results in Physics 31 (2021) 104874

Contents lists available at ScienceDirect

Results in Physics

journal homepage: www.elsevier.com/locate/rinp

Dynamic susceptibility of permalloy wire-tube nanostructures

E. Saavedra [a], N. Vidal-Silva [b,*], J. Escrig [a,c]

[a] Departamento de Física, Universidad de Santiago de Chile (USACH), 9170124 Santiago, Chile
[b] Departamento de Ciencias Físicas, Universidad de La Frontera, Casilla 54-D, 4811186 Temuco, Chile
[c] Center for the Development of Nanoscience and Nanotechnology (CEDENNA), 9170124 Santiago, Chile

ARTICLE INFO

Keywords:
Wire-tube
Nanocylinders
Nanowires
Spin-waves
Dynamical response

ABSTRACT

In this work, we have theoretically explored the spin-waves modes that can be excited in cylindrical nanostructures with wire-tube morphology. Using micromagnetic simulations, we have found up to 5 resonance modes whose existence and position depend on the geometric parameters of the nanostructure. The lower and higher frequency modes remain invariant in their position as a function of the size of the tube segment hole, although their intensity increases as the length of the wire segment increases. Other modes vary in their frequency, even producing a crossover between them. Finally, we found that the number and amplitude of the reported spin-wave modes have a complex dependence on the geometry of the system, converting the wire-tube nanostructure into a promising piece for potential magnonic devices.

Introduction

Cylindrical magnetic nanostructures configure a valuable block to build new technologies such as sensors, logic and spintronic devices, as well as information storage systems, mainly due to the exploitation of the height, which adds a new degree of freedom to the system if we compare them with the usual spherical nanoparticles [1–3]. The main advantage of these cylindrical nanostructures is that magnetization, in the absence of crystalline anisotropy and external magnetic fields, will try to point along the axis of the cylinder due to the magnetostatic field, which defines the shape anisotropy of the nanostructure. In this way, the height of the cylindrical nanostructures makes it possible to overcome the superparamagnetic limit that affects spherical nanoparticles.

The magnetic properties of cylindrical nanostructures are closely related both to their magnetic and geometric parameters [4,5]. For instance, it has been theoretically and experimentally shown that the magnetic ground state of magnetic nanotubes can be tuned simply by changing their geometric parameters [6,7]. Specifically, the reported states are those so-called ferromagnetic in-plane, where the magnetic moments point perpendicular to the axial axis; ferromagnetic out-of-plane, where the magnetic moments point along the axial axis; and the vortex configuration, where the magnetic moments lie tangent to the cylinder surface in the plane parallel to its base. Obviously if we add magnetocrystalline anisotropies or external magnetic fields other magnetic configurations can be stabilized [8,9].

Furthermore, the magnetization reversal processes also depend on the geometric parameters of the nanostructures, as has been shown, for example, in magnetic nanotubes, where depending on the radii involved, the system can reverse its magnetization by nucleating the vortex or transverse domain walls, which then propagate from the ends of the nanostructure towards its center [10–12]. Similar behaviors have been observed in magnetic nanowires, where stabilized magnetic configurations and magnetization reversal mechanisms also have a strong dependence on their geometric parameters [13,14]. In this way, the static magnetic properties of cylindrical nanostructures can be adjusted by varying the geometry of the system, which essentially implies a change in the shape anisotropy of the system [15–17].

On the other hand, the dynamic properties of cylindrical nanostructures have also been intensely studied. In particular, the dynamic susceptibility of nanowires and nanotubes shows two main peaks at different frequencies [18–20]. The low energy mode stands for the excitation of spins located at the ends of the nanostructure, which is usually called the *edge mode*. In contrast, the higher energy mode corresponds to the dynamical response of the spins primarily located in the central zone of the nanostructure. It is usually called the *bulk mode*. This feature allows proposing these nanostructures as spin-wave filters, where the desired mode is activated according to the excitation frequency [21].

A particular cylindrical nanostructure that mixes features of nanotubes and nanowires is the wire-tube nanostructure that corresponds to a tube segment joined to a wire segment (see Fig. 1). These nanostructures have recently been studied both from a theoretical and experimental point of view, finding new magnetic properties [22–24].

* Corresponding author.
E-mail address: nicolas.vidal@ufrontera.cl (N. Vidal-Silva).

https://doi.org/10.1016/j.rinp.2021.104874
Received 2 September 2021; Accepted 29 September 2021
Available online 15 October 2021

For example, it may happen that the tube segment exhibits a lower coercivity than the wire segment, producing a hysteresis curve that accommodates a well-defined step [25]. For magnetic fields within the range of the step, we obtain a nanostructure with two opposing magnetic domains, obtaining an antiparallel configuration, separated by a vortex domain wall, which has been proposed for a pseudo on/off transistor device [26]. Furthermore, the tube segment can revert its magnetization through nucleation and propagation of a vortex domain wall, while the wire segment does so through a transverse domain wall [27]. These novel properties emerge from the combined effect of the magnetostatic field generated by both the tube segment and the wire segment [28,29]. In this way, its static properties strongly depend on the geometric parameters that characterize both sections.

The natural next step is to study the dynamic response of wire-tube nanostructures when a weak magnetic pulse is applied. This is an important problem that we have to face because although the static properties of cylindrical nanostructures are enriched by the wire-tube shape, it is not clear whether the dynamic properties inherit this behavior and exhibit new properties attributable to the combined wire-tube system. Thus, in this paper, we investigate the dynamic response of cylindrical wire-tube nanostructures when a weak magnetic pulse is applied perpendicular to the axis of the cylinder. We tackled this problem by performing micromagnetic simulations of 1 μm long wire-tube nanostructures with an external radius of 15 nm. To explore the incidence of geometric parameters on the dynamic response of the system, we have considered permalloy (Py) nanostructures because it is a soft material with negligible magnetocrystalline anisotropy, so the magnetic properties will depend only on its shape anisotropy [30].

Micromagnetic simulations and method

As mentioned above, to study the dynamic response of wire-tube nanostructures when a weak magnetic pulse is applied, we perform micromagnetic simulations using the free-licensed OOMMF code [31]. We consider a permalloy nanostructure characterized by a stiffness constant $A = 13 \times 10^{-12}$ J/m and a saturation magnetization $M_s = 800 \times 10^3$ A/m. The wire-tube nanostructure is defined by its external radius $R = 15$ nm, internal radius a (in the tube segment) and its total length $L = 1$ μm. This length includes the wire segment with length h and the tube segment with length $L - h$, as depicted in Fig. 1. It is convenient to define the ratio $\beta = a/R$ to parametrize the tube segment. In this way, $\beta = 0.0$ represents a solid nanowire, while $\beta \to 1.0$ corresponds to an ultra-narrow tube. Similarly, we define the ratio $\eta = h/L$ to parametrize the portion of the wire-tube nanostructure that corresponds to a tube or a wire segment. Thus, a magnetic tube is represented by $\eta = 0.0$, a magnetic wire by $\eta = 1.0$, while other values of η represent a wire-tube nanostructure. For all our calculations we have varied β ranging from 0.0 up to 0.9 in steps of 0.1, and η ranging from 0.0 up to 1.0 in steps of 0.05. Finally, the system is discretized in cubic cells of $1.5 \times 1.5 \times 5$ nm^3 (the later along the nanostructure axis).

To obtain the dynamic response of the wire-tube nanostructure, we use the Ringdown method to simulate the FMR spectrum [32], a method that considers the following steps: First, the minimum energy configuration of the system is obtained by minimizing the total energy $E_m = E_{ex} + E_{demg}$, corresponding to the exchange and dipolar energy, respectively, thus obtaining the metastable states displayed in Fig. 2 for selected values of η and β. From this figure, we can see that the metastable states correspond to a configuration where the magnetic moments point almost uniformly along the nanostructure axis. However, small disturbances can be seen both at the ends of the nanostructure and in the transition zone between the wire and tube segments, which can be attributed to the demagnetizing field produced by the magnetic charges in these zones.

Once we have obtained the metastable states, this equilibrium configuration is excited with a small microwave field of the form $\mathbf{h}(t) = 1000\exp(-10^9 t)\hat{\mathbf{x}}$ A/m [19,33]. The dynamical response is obtained by numerically solving the Landau–Lifshitz–Gilbert (LLG) equation

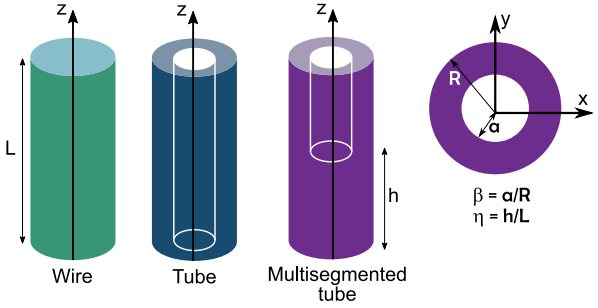

Fig. 1. Schematic representation of the studied system. From left to right: a solid nanowire, a nanotube, and a wire-tube nanostructure.

$$\dot{\mathbf{m}} = -\gamma \mathbf{m} \times \mathbf{H}_{\text{eff}} + \alpha \mathbf{m} \times \dot{\mathbf{m}}, \tag{1}$$

with γ the gyromagnetic ratio, α the phenomenological Gilbert damping, which for our calculation was chosen as $\alpha = 0.015$, value that is lower than 0.2 commonly used for a dynamic study [34], and the effective field $\mathbf{H}_{\text{eff}}$ defined as $\mu_0 \mathbf{H}_{\text{eff}} = -\delta E_m[\mathbf{M}]/\delta \mathbf{M}$ that now considers the additional Zeeman term coming from the application of the microwave field. The amplitude of this pulse must be small enough to keep the system in the linear response regime [35]. The temporal evolution of the magnetization under the action of the exciting field is collected for 4 ns recording the magnetization configuration at uniform time intervals of 1 ps allowing a spectral resolution of 0.25 GHz. Then, the small exciting magnetic field $h(t)$ and the magnetization distribution $M(\mathbf{r}, t)$ are transformed to the frequency domain $[h(\omega, M(\omega))]$ using the fast Fourier transform (FFT) method. The dynamic susceptibility $\chi(\omega)$, which corresponds to the imaginary part of the magnetic susceptibility, is calculated as $\chi(\omega) = M(\omega)/h(\omega)$ [36].

Results and discussion

In Fig. 3 we show the dynamic susceptibility for $\eta = 0.5$ and selected values of β, where we identify the presence of 5 main peaks, which depends directly on the parameters β and η as we will show below. Fig. 3(a) corresponds to $\beta = 0.2$ and $\eta = 0.5$. In this case, only three peaks appear, namely, peaks 1, 2, and 5. Recall that β controls the transition between a solid wire and one with a tube section. Therefore, $\beta = 0.2$ corresponds to a nearly solid nanowire. Note that the peaks 1 and 2 stand for low energy and small amplitude modes, but the peak 5 corresponds to a higher energy mode with a bigger amplitude. Thus, the mode 5 must correspond to a coherent precession of many spins in the system. Next, Fig. 3(b) shows the case for $\beta = 0.4$ which also presents the same two lowest energy peaks 1 and 2, as the highest energy peak 5, but now peaks 3 and 4 appear that were absent in the $\beta = 0.2$ case. Similar results can be seen in the cases $\beta = 0.5$ and $\beta = 0.6$, as seen in Figs. 3(c)–(d), where the most remarkable effect is that peaks 3 and 4 move towards lower frequencies while peak 2 moves towards higher frequencies, producing an overlap and transition of peaks 2 and 3 for $\beta = 0.7$, as seen in Fig. 3(e). Finally, Fig. 3(f) shows a wire-tube nanostructure with a very thin tube segment, where the peaks 2 and 3 are completely stabilized in their new characteristic frequencies, while peaks 1 and 5 remain in their same positions regardless of the β value.

The results presented in Fig. 3 can be summarized by computing the frequency of the resonant modes as a function of β, as shown in Fig. 4(b). For completeness, Fig. 4(a) and (c) shows the resonant frequency modes for the cases $\eta = 0.25$ and $\eta = 0.75$, respectively (further values of η can be found in supplementary information). We identify the presence of five resonant peaks according to the value of β. Specifically, for small β values ($\beta < 0.3$), there are only three modes: modes 1, 2, and 5, although modes 1 and 2 are quite weak.

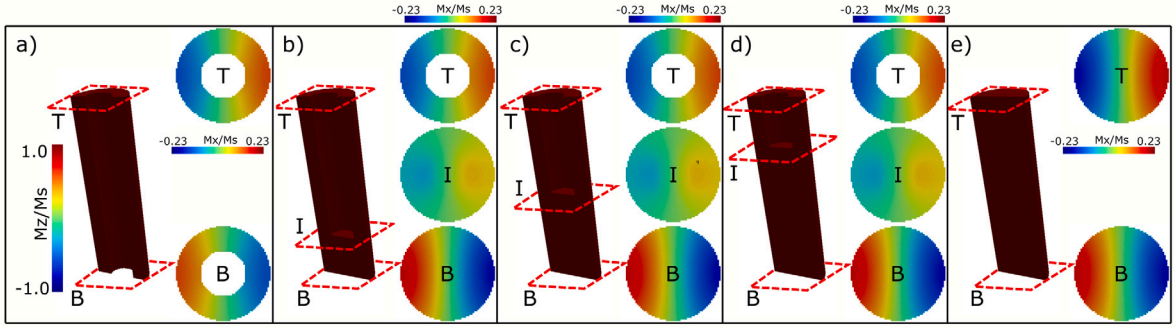

Fig. 2. Metastable states hosted in a wire-tube nanostructure with $\beta = 0.5$ and (a) $\eta = 0.0$, (b) $\eta = 0.25$, (c) $\eta = 0.5$, (d) $\eta = 0.75$ and (e) $\eta = 1.0$. The vertical colored bar represents the magnitude of the $z-$component of the magnetization. The horizontal colored bar represents the magnitude of the $x-$component of magnetization at the ends of the nanostructure and at the intersection between both segments. (For interpretation of the references to color in this figure legend, the reader is referred to the web version of this article.)

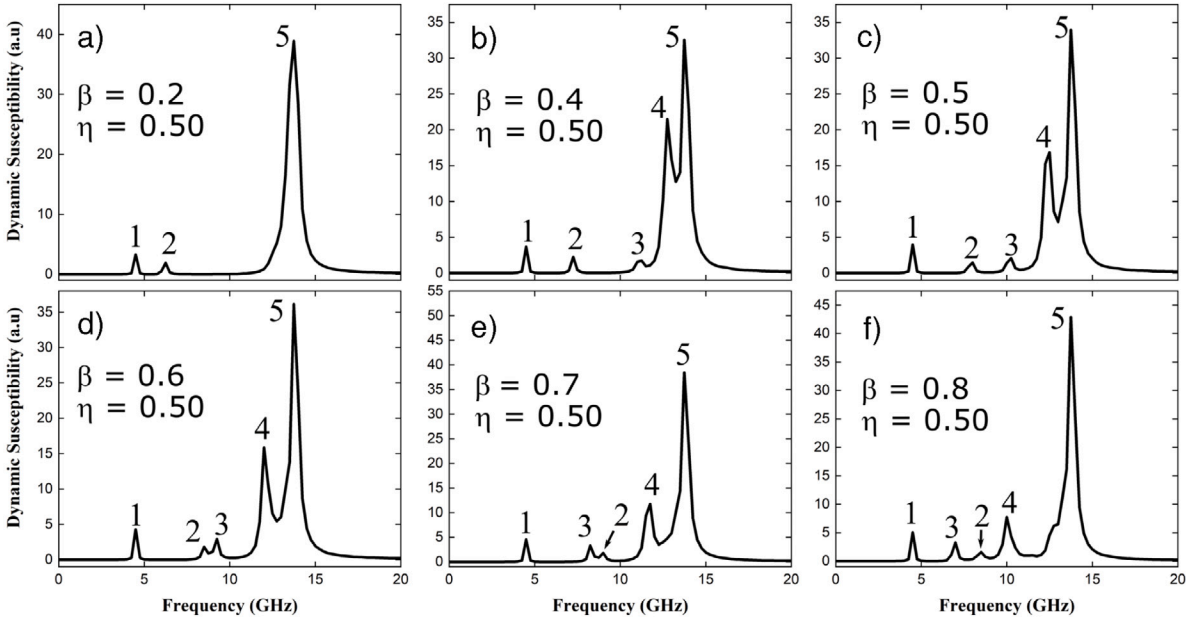

Fig. 3. Dynamic susceptibility of a 1 μm long nanostructure with an external radius of 15 nm for $\eta = 0.5$ and (a) $\beta = 0.2$, (b) $\beta = 0.4$, (c) $\beta = 0.5$, (d) $\beta = 0.6$, (e) $\beta = 0.7$ and (f) $\beta = 0.8$.

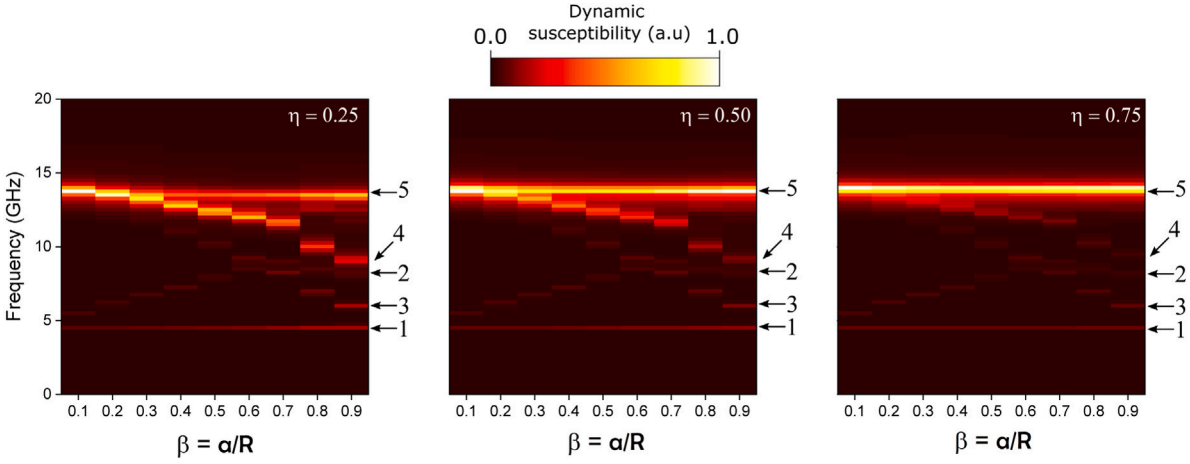

Fig. 4. Frequency of the resonant modes as a function of β for (a) $\eta = 0.25$, (b) $\eta = 0.50$ and (c) $\eta = 0.75$. The intensity of these peaks is represented by the dynamic susceptibility and its corresponding color bar. (For interpretation of the references to color in this figure legend, the reader is referred to the web version of this article.)

However, new modes appear (peaks 3 and 4) when we increase the β value, implying that the tube segment thins its walls. An important fact occurs for $\beta = 0.6$, where modes 2 and 3 intersect at the same frequency value. This crossover is satisfied for all the η values investigated. In fact, the number of resonant modes does not depend on this η parameter (see the related discussion in supplementary material) but, in fact, this

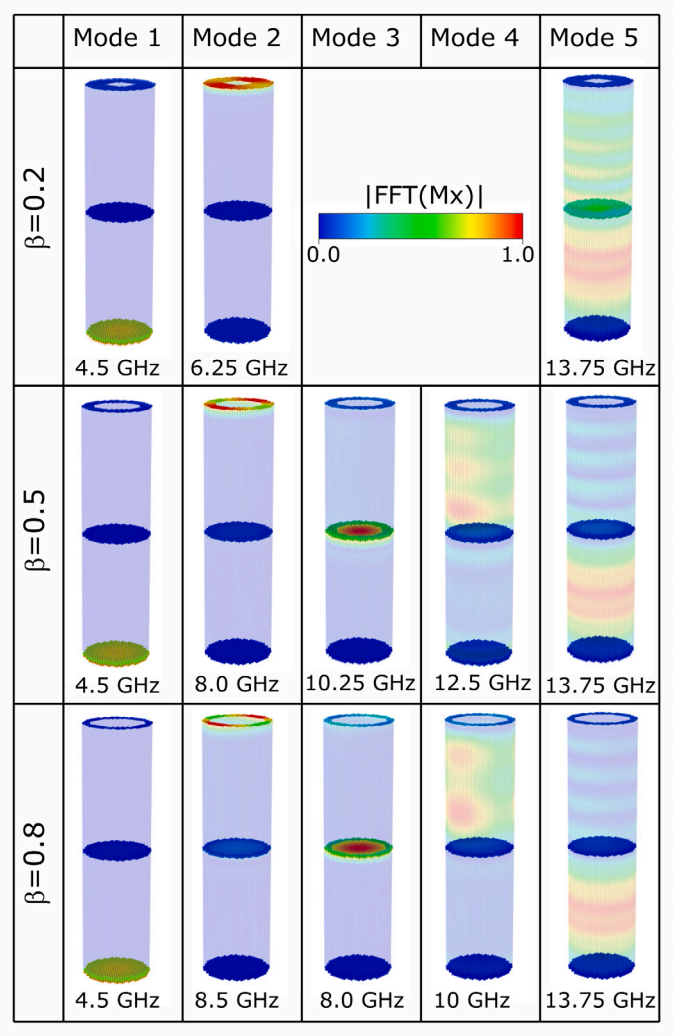

Fig. 5. Spatial distribution of the excited spin-waves modes when applying the small microwave magnetic pulse. The columns correspond to the five reported modes, while the rows have distinct values of β. The color code establishes the amplitude of the FFT employed on the $x-$component of the magnetization field. The red color implies higher spin amplitude, while the blue color means zero spin amplitude. (For interpretation of the references to color in this figure legend, the reader is referred to the web version of this article.)

parameter only has an effect on the amplitude of the resonant modes, that is, on the number of magnetic moments that are excited at a certain frequency, but not in the value of this frequency, as seen by the color intensity in Fig. 4.

To know the origin of the resonant modes and better understand the behavior that this system has when changing the geometrical parameters, in Fig. 5 we have represented the spatial distribution of the resonant modes for $\eta = 0.5$ and selected values of β. The rows correspond to the values of β, while the columns are the five distinct modes found above. Note that modes 1 and 2 are always present, and they are essentially the reported edge modes that emerge from the excitation of spins located mainly at the free ends of the wire-tube nanostructure. For $\beta = 0.2$, the next higher energy mode only appears at the highest frequency reported, namely, mode 5 at 13.75 GHz, whose origin lies in the excitation of most spins located within the whole bulk structure. This mode is the well reported bulk mode. Next, the case $\beta = 0.5$ shows all reported peaks. As stated above, modes 1 and 2 are present too, but now modes 3, 4 and 5 appears. Mode 3 corresponds to the excitation of spins located at the transition zone between the tube and wire section. Since β controls the hole size in the tube section, this mode is absent for $\beta = 0.2$ because there is more magnetic material so that its excitation demands higher energies. In the case $\beta = 0.5$, the hole is bigger than the previous case, so more spins are located at the inner surface that can be excited easier. Following the same idea, the next higher energy mode, mode 4, corresponds to a bulk mode originated from the spin excitation of the tube section. Finally, the entire structure, although more pronounced the wire section, is coherently excited, activating the mode 5. Note that $\beta = 0.8$ corresponds to a wire-tube nanostructure with a thin tube section. This has several consequences on the excitation modes because, as we argued above, the high population of surface spins favors the activation of the spin-wave modes. In fact, mode 2 that in the previous cases is purely originated at the free ends of the nanostructure now also comprises a weak spin excitation at the interface between the tube and wire section. More importantly, mode 3 that corresponds to the excitation of spins located at the transition zone is now of lower energy than mode 2. This is a consequence of considering a thinner tube section, and the effect is less noticeable as long as the portion of the wire section is smaller, i.e., when increasing η (see Fig. 4 and the supplementary material). The last two modes behave in the same way as the case $\beta = 0.5$, demonstrating that the importance of modifying the β parameter is reflected mainly in edge-like modes while the bulk modes remain intact.

Conclusions

We have studied the resonant modes in a wire-tube nanostructure as a function of the geometric parameters of the system. We found

that, in general, for nanostructures with a thin tube section, several spin waves modes can be excited, which progressively turn off if the tube section becomes thicker. We explain this in terms of the amount of magnetic material available to be excited. In this sense, thinner tube sections promote an easier spin excitation, so it could be useful when designing nanodevices as magnonic filters. Interestingly, we have found that the height of the wire subsection has no critical consequences on the number of resonant peaks, but it does on the amplitude of the spin waves modes, which opens the possibility of exploiting such features as modulated signals. Additionally, we predict a crossing mode when changing the wall width of the tube section, which allows controlling the energy at which the spin-waves modes are excited. Finally, we demonstrated that it is possible to add new degrees of freedom by geometrically changing the morphology of the wire-tube nanostructure, as evidenced by the new spin-waves modes that appear for specific geometrical parameters, which are easily feasible with the current experimental techniques.

CRediT authorship contribution statement

E. Saavedra: Conceptualization, Software, Visualization, Formal analysis. **N. Vidal-Silva:** Conceptualization, Methodology, Formal analysis, Writing – original draft. **J. Escrig:** Conceptualization, Resources, Formal analysis, Writing – original draft.

Declaration of competing interest

The authors declare that they have no known competing financial interests or personal relationships that could have appeared to influence the work reported in this paper.

Acknowledgments

This work was supported by Fondecyt Postdoctorado, Chile 3190264, Fondecyt Regular, Chile 1200302 and Basal project, Chile AFB180001.

Supplementary data

Supplementary material related to this article can be found online at https://doi.org/10.1016/j.rinp.2021.104874. There, the dynamic susceptibility, frequency of the resonant modes, and the origin of such modes for different values of β and η are discussed.

References

[1] Cowburn RP, Welland ME. Science 2000;287:1466.
[2] Vazquez M, editor. Magnetic nano- and microwires. Cambridge: Woodhead Publishing; 2015.
[3] Parkin S, Yang SH. Nat Nanotechnol 2015;10:195.
[4] Landeros P, Escrig J, Altbir D, Laroze D, d'Alburqueque e Castro J, Vargas P. Phys Rev B 2005;71:094435.
[5] Staño M, Fruchart Olivier. Handbook of magnetic materials, Vol. 27. 2018, p. 155–267.
[6] Escrig J, Landeros P, Altbir D, Voge EE, Vargas P. J Magn Magn Mater 2007;308:233.
[7] Ye Yixing, Geng Baoyou. Crit Rev Solid State Mater Sci 2012;37:75–93.
[8] Escrig J, Landeros P, Altbir D, Vogel EE. J Magn Magn Mater 2007;310:2448.
[9] Chen AP, Guslienko KY, Gonzalez J. J Appl Phys 2010;108:083920.
[10] Landeros P, Allende S, Escrig J, Salcedo E, Altbir D, Vogel EE. Appl Phys Lett 2007;90:102501.
[11] Escrig J, Bachmann J, Jing J, Daub M, Altbir D, Nielsch K. Phys Rev B 2008;77:214421.
[12] Albrecht O, Zierold R, Allende S, Escrig J, Patzig C, Rauschenbach B, Nielsch K, Gorlitz D. J Appl Phys 2011;109:093910.
[13] Lavin R, Denardin JC, Escrig J, Altbir D, Cortes A, Gomez H. J Appl Phys 2009;106:103903.
[14] Raviolo S, Tejo F, Bajales N, Escrig J. Mater Res Express 2018;5:015043.
[15] Escrig J, Lavin R, Palma JL, Denardin JC, Altbir D, Cortes A, Gomez H. Nanotechnology.
[16] Sui YC, Skomski Ralph, Sorge Kory D, Sellmyer David J. Appl Phys Lett 2004;84:1525–7.
[17] Fernandez-Roldan J-A, Chrischon D, Dorneles LS, Chubykalo-Fesenko O, Vazquez M, Bran C. Nanomaterials 2018;8:692, 19 (2008) 075713.
[18] Dao N, Donahue MJ, Dumitru I, Spinu L, Whittenburg SL, Lodder JC. Nanotechnology 2004;15:S634.
[19] Liu R, Wang J, Liu Q, Wang H, Jiang C. J Appl Phys 2008;103:013910.
[20] Yang J, Kim J, Kim B, Cho Y-J, Lee J-H, Kim S-K. J Appl Phys 2018;123:033901.
[21] Saavedra E, Saez G, Diaz P, Cisternas E, Vogel EE, Escrig J. AIP Adv 2019;9:065007.
[22] Arshad MS, Pecko D, Sturm S, Escrig J, Komelj M, McGuiness PJ, Kobe S, Rozman KZ. IEEE Trans Magn 2014;50:2302904.
[23] Arshad MS, Sturm S, Zavasnik J, Espejo AP, Escrig J, Komelj M, McGuiness PJ, Kobe S, Rozman KZ. J Nanopart Res 2014;16:2688.
[24] Salazar-Aravena D, Escrig J, Laroze D. J Magn Magn Mater 2020;497:165935.
[25] Salazar-Aravena D, Corona RM, Goerlitz D, Nielsch K, Escrig J. J Magn Magn 2013;346:171.
[26] Espejo AP, Vidal-Silva N, Lopez-Lopez JA, Goerlitz D, Nielsch K, Escrig J. Appl Phys Lett 2015;106:132405.
[27] Salazar-Aravena D, Palma JL, Escrig J. Mater Res Express 2014;1:026112.
[28] Salazar-Aravena D, Palma JL, Escrig J. J Appl Phys 2015;117:193905.
[29] Riveros A, Salazar-Aravena D, Escrig J. J Magn Magn Mater 2017;428:452.
[30] Gerardin O, Youssef JB, Le Gall H, Vukadinovic N, Jacquart PM, Donahue MJ. J Appl Phys 2000;88:5899.
[31] Donahue MJ, Porter DG. OOMMF user's guide, Version 1.2 a3. 2002, http://math.nist.gov/oommf.
[32] Baker A, Beg M, Ashton G, Albert M, Chernyshenko D, Wang W, Zhang S, Bissoti MA, Franchin M, Hu CL, Stamps R, Hesjedal T, Fangohr H. J Magn Magn Mater 2017;421:428.
[33] Peng Y, Zhao GP, Morvan FJ, Wu SQ, Yue M. J Magn Magn Mater 2017;422:57.
[34] Russek SE, Kaka S, Donahue MJ. J Appl Phys 2000;87:7070.
[35] Wagner K, Stienen S, Farle M. e-print arXiv:1506.05292v1 [physics.comp-ph].
[36] Wen-Bing C, Man-Gui H, Hao Z, Yu O, Long-Jiang D. Chin Phys B 2010;19:087502.